Modeling of field-aligned electron bursts by dispersive Alfvén waves in the dayside auroral region

Yi-Jiun Su,[1] Samuel T. Jones,[2] Robert E. Ergun,[1] and Scott E. Parker[2]

Received 4 December 2003; revised 3 August 2004; accepted 12 August 2004; published 2 November 2004.

[1] A linear, one-dimensional gyrofluid code including electron inertia, electron pressure gradient, and finite ion gyroradius effects is applied to an inhomogeneous dayside auroral field line to determine the characteristics of propagating Alfvén waves with small perpendicular wavelengths. Test particles are then used to study the behavior of both magnetosheath (100 eV) and background ionospheric electrons (2 eV) under the influence of dispersive Alfvén waves. Although the test particle approach is not self-consistent, the gyrofluid/test particle simulation is able to reproduce many of the features observed by low-altitude satellites. The test particle simulations verify results from previous studies, such as reproducing electron energy and pitch-angle dispersions, and in doing so, validate the approach. The test particle simulations also show how resonant particles can lead to low-energy field-aligned electron bursts that are commonly observed in the dayside auroral region. The new results in this study reveal the plasma conditions necessary for electron resonance. We show that an increased mass density (significant O^+ density) in the acceleration region is an essential prerequisite to generate an electron burst. The primary effect of the O^+ is to decrease the phase speed of the Alfvén wave. Furthermore, the full gyrokinetic effects of the O^+ act to produce a region in which the Alfvén speed profile is gradually slowing, which allows electrons remaining within the wave to lower altitudes. In these electron bursts, the energy gain experienced by the majority of electrons ranges from tens to hundreds of eV. The trapping occurs if the parallel electric field is substantial enough ($\sim$0.2 mV/m) in the acceleration region to accelerate the background electrons. An integrated energy flux of accelerated electrons is estimated to be 3 erg s^{-1} cm^{-2}, about 20% of the Alfvén wave Poynting flux. *INDEX TERMS:* 2431 Ionosphere: Ionosphere/magnetosphere interactions (2736); 2451 Ionosphere: Particle acceleration; 2487 Ionosphere: Wave propagation (6934); 2483 Ionosphere: Wave/particle interactions; *KEYWORDS:* electron acceleration, Alfvén wave propagation, magnetosphere-ionosphere coupling, particle acceleration

Citation: Su, Y.-J., S. T. Jones, R. E. Ergun, and S. E. Parker (2004), Modeling of field-aligned electron bursts by dispersive Alfvén waves in the dayside auroral region, *J. Geophys. Res.*, *109*, A11201, doi:10.1029/2003JA010344.

1. Introduction

[2] Shear Alfvén waves represent perturbations of the perpendicular electric and magnetic field traveling in the direction of the ambient magnetic field. In ideal magnetohydrodynamic (MHD) theory, these Alfvén waves have no field-aligned electric field component and therefore provide no parallel acceleration to particles. However, a parallel electric field can be produced by low-frequency dispersive Alfvén waves ($\omega < \omega_{ci}$, where ω_{ci} is the ion gyrofrequency) when the parallel electric force is balanced by the electron inertia (i.e., inertial Alfvén wave [*Goertz and Boswell*, 1979]) or the electron pressure gradient (i.e., kinetic Alfvén wave [*Hasegawa*, 1976]) [*Stasiewicz et al.*, 2000, and references therein]. Hence a dynamic model including both inertial and kinetic effects should be considered when studying Alfvén waves in the magnetosphere-ionosphere (M-I) coupling.

[3] Various numerical investigations have been performed with models including both electron inertia and pressure gradient effects in an effort to study dispersive field line resonances with reduced MHD equations [*Rankin et al.*, 1999; *Lu et al.*, 2003] or reduced two-fluid equations [*Streltsov and Lotko*, 1995; *Streltsov et al.*, 1998]. Such models were primarily designed to study standing Alfvén waves along closed field lines. Although field line resonances are not studied here, the behavior of Alfvén waves propagating through the transition region (between the kinetic and inertial regimes) as modeled by the gyrofluid code used in this investigation is similar to those reported in previous studies. This paper goes beyond previous investigations to demonstrate the behaviors of electrons and waves in the O^+ dominated acceleration region.

[4] Other models have been employed to explain the acceleration of electrons by both linear Alfvén waves [e.g.,

[1]Laboratory for Atmospheric and Space Physics, University of Colorado, Boulder, Colorado, USA.
[2]Center for Integrated Plasma Studies, University of Colorado, Boulder, Colorado, USA.

0148-0227/04/2003JA010344$09.00

Nakamura and Tamao, 1989; *Kletzing*, 1994; *Streltsov and Lotko*, 1995] and nonlinear Alfvén waves [e.g., *Hui and Seyler*, 1992; *Knudsen*, 1996; *Seyler et al.*, 1998; *Clark and Seyler*, 1999; *Génot et al.*, 2001]. Some authors have made an effort to evaluate their simulation results through direct comparison with observations. In one of these studies, *André and Eliasson* [1995] were able to reproduce electron conics through interactions with broadband parallel electric field fluctuations. Alternatively, *Thompson and Lysak* [1996] were able to do the same through interactions with inertial Alfvén waves. By using one-dimensional (1-D) MHD model including an electron inertial correction, *Chaston et al.* [2002a] were able to replicate some of the observed features on the nightside polar cap boundary region. Among these features were waveforms and frequency-dependent field structures and electron distribution functions of the ionospheric Alfvén resonator [*Lysak*, 1991, 1993].

[5] A significant amount of observational evidence indicates that Alfvén waves play a strong role in electron acceleration in the dayside auroral/cusp regions. These electrons show many of the same signatures as in the nightside but are dominated by field-aligned bursts. Electric field observations from the Viking satellite have shown that the cusp region is characterized by irregular and spiky electric fields [*Marklund et al.*, 1990]. *Matsuoka et al.* [1993] indicated that the irregular fluctuations of electric field observed by EXOS-D are considered to be Alfvén waves and suggested that the Alfvén waves are generated in association with the particle injection into the magnetosphere when reconnection occurs. FAST observations reveal highly structured electrons in the cusp region associated with intense electric field variations [*Pfaff et al.*, 1998; *Su et al.*, 2001], which are related to propagating Alfvén waves [*Chaston et al.*, 1999]. On the basis of observations from the Freja satellite, *Andersson et al.* [2002] reported that two distinct electron signatures (field-aligned and time-dispersive properties) are associated with the propagating Alfvén wave in the dayside auroral region. With the assumption of a simple potential profile, *Andersson et al.* [2002] were able to reproduce the energy-dispersive signature by tracing particle trajectories. The pitch-angle dispersion was also reproduced by Andersson et al. when the magnetic mirror effect was included in their test particle tracing. By varying the magnetic field and density along the flux tube, *Kletzing and Hu* [2001] produced a time-dispersed electron signature with the energy up to $\sim$1 keV from their Alfvén wave model. With a 1-D MHD code including inertial corrections for propagating shear Alfvén waves in the dayside auroral oval with test particles, *Chaston et al.* [2000] obtained a broad crescent-shaped electron feature above 200 eV in a plot of pitch angle versus energy, as well as a field-aligned electron burst with the highest energy reaching $\sim$600 eV. In this article we consider the effects of heavy ions (O^+) and demonstrate that an enhanced density at low altitudes plays a significant role in Alfvén wave dynamics. The lower phase speed enhances resonant electrons, allowing us to reproduce electron bursts.

[6] This paper focuses on Alfvén wave related electron signatures and electric and magnetic field fluctuations seen by the FAST satellite in the dayside auroral regions. We not only reproduce the energy and pitch angle dispersive electron signatures but also explore the plasma conditions required to generate field-aligned electron bursts. The propagation of dispersive Alfvén waves is performed by a one-dimensional gyrofluid code [*Jones*, 2004; *Jones and Parker*, 2003] in an inhomogeneous plasma including electron, H^+, and O^+ species. A test particle tracing method is employed to examine the response of electrons to propagating Alfvén waves. An example of electron signatures observed by the FAST satellite is presented in section 2. The model used in this paper is described in section 3. Simulation results from our study are shown in section 4. Finally, section 5 contains discussions and conclusions drawn from these model results.

2. Motivation: FAST Observations

[7] This numerical study is motivated by electron signatures observed by the FAST satellite. An example is shown in Figure 1 when the FAST satellite passed through the dayside auroral region from 0833:25 to 0833:28.5 UT on 17 July 1997. Figure 1a shows the observed electric fields along the spacecraft trajectory that are nearly perpendicular to the local magnetic field. Magnetic field perturbations in the direction perpendicular to both the spacecraft trajectory and the local magnetic field are plotted in Figure 1b. The ratio of electric and magnetic field perturbations is approximately 10^4 km s^{-1} at $\sim$0833:27 UT, which is on the same order as the local Alfvén speed. Figures 1c and 1d are the electron energy and pitch-angle spectrograms, respectively, where the logarithm of the energy flux is color-coded according to the color bar.

[8] Two distinct features are marked by the arrows: a time-dispersive electron signature and a field-aligned electron burst. Similar features observed by the Freja satellite were presented by *Andersson et al.* [2002, Figure 2]. Both time-dispersion and burst signatures are believed to associate with propagating Alfvén waves [*Andersson et al.*, 2002]. Although the time dispersion signature is primarily in the downward direction toward the ionosphere (0° in Figure 1d), the pitch angle of electrons are broadened with increasing time (a bow shape in green color outlined by a black dashed curve in Figure 1d). This signature is more clearly shown in distribution functions of Figures 1e–1h, where the negative (positive) parallel velocity is the direction toward (away from) the ionosphere. Time-dispersive electrons have been reproduced by test particles from previous studies [*Kletzing and Hu*, 2001; *Andersson et al.*, 2002]. In this study, we are able to verify these earlier results as applied to the dayside aurora and, in doing so, validate our model.

[9] Field-aligned electron bursts are the commonly detected signature in the auroral oval. They are also referred to as low-energy field-aligned electron bursts or suprathermal electron bursts [e.g., *Hoffman and Evans*, 1968; *Johnstone and Winningham*, 1982; *McFadden et al.*, 1986; *Clemmons et al.*, 1995]. These electrons show characteristics that are narrow in pitch angle (field-aligned toward ionosphere) and broad in energy bins (tens to hundreds of eV). Supratheramal electron bursts are also observed together with an inverted-V structure in the nightside aurora

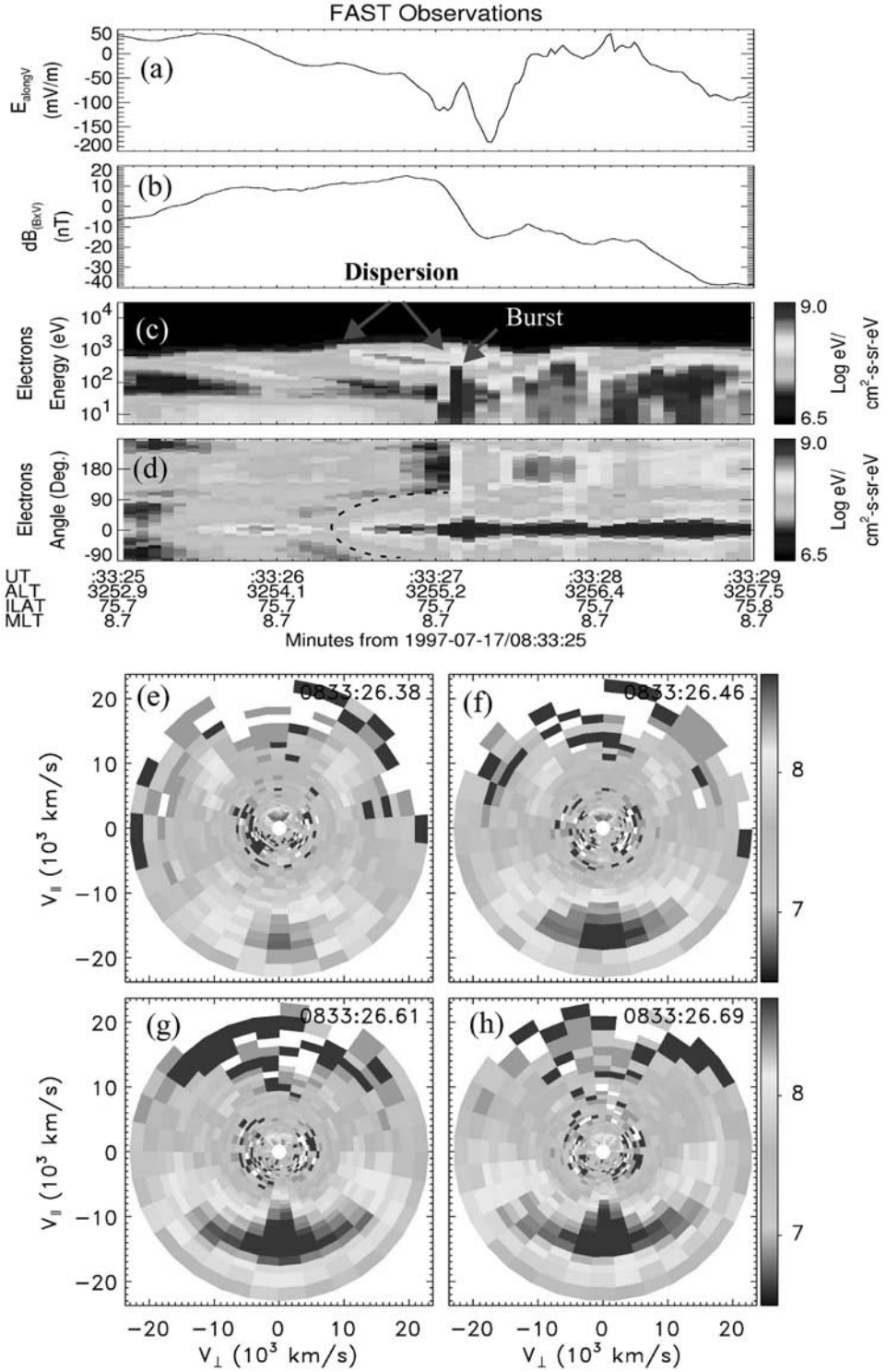

Figure 1. FAST observations of the dayside auroral region on 17 July 1997. (a) Perpendicular electric fields. (b) Perpendicular magnetic fields. (c) Electron energy-time spectrogram. (d) Electron angular time spectrogram, where 0° (180°) indicates the direction parallel (antiparallel) to the local magnetic field. Four snapshots of the electron distribution functions are displayed in Figures 1e–1h during times when the energy-time dispersion signature was observed. The vertical and horizontal axes are parallel and perpendicular velocity with respect to the local magnetic field, where negative velocity is the direction toward the ionosphere. The color represents electron energy fluxes according to the color bar on the right. See color version of this figure at back of this issue.

region. *Chaston et al.* [2002b] applied a time-varying potential derived from observed electric fields and reproduced those electron signatures in a nightside inverted-V region. In the dayside, electron bursts are observed without the presence of inverted-V structures. The focus of this paper is to more fully understand the plasma conditions necessary to generate these electron bursts from our linear Alfvén wave model.

3. Model Description

3.1. Gyrofluid Code

[10] For the purpose of this study, a linear one-dimensional gyrofluid model [*Jones and Parker*, 2003; *Jones*, 2004] is adopted to simulate the propagating Alfvén wave on a dayside auroral flux tube. This gyrofluid code includes both drift-fluid electrons and gyrofluid ions and also allows for modeling of full finite gyroradius, electron pressure gradient, and electron inertia effects. The derivation of the gyrofluid equations is adapted from *Beer and Hammett* [1996]. The finite Larmour radius effects for electrons are neglected. The density relation for the electrons and ions is obtained from the zero moment of the kinetic equation (i.e., the continuity equation):

$$\frac{\partial \delta n_s}{\partial t} = -u_{\|s}\frac{\partial n_s}{\partial z} - n_s\frac{\partial u_{\|s}}{\partial z} + u_{\|s}n_s\frac{1}{B}\frac{\partial B}{\partial z}, \tag{1}$$

where n_s represents the density for each particle species s. Three particle species (e^-, H^+, and O^+) are considered in our simulation, where $n_e = n_H + n_O$. Here δn_s is the density perturbation, $u_{\|s}$ is the parallel velocity, and B is the magnetic field. A simple dipole magnetic field is assumed for this study.

[11] The ion gyroaveraged guiding center density, $\overline{n_i}$, is obtained from the Padé approximation $\overline{n_i} = n_i\Gamma_o^{1/2} \approx n_i/(1 + b_i/2)$. $\Gamma_o(b_i) = I_o(b_i)e^{-b_i}$, where I_o is the first modified Bessel function, and $b_i = k_\perp^2\rho_i^2 = k_\perp^2 T_i m_i (eB)^{-2}$. Here ρ_i is the ion gyroradius.

[12] The momentum relation of the first gyrofluid moment can be described as

$$\frac{\partial n_s u_{\|s}}{\partial t} = -B\frac{\partial}{\partial z}\left(\frac{p_{\|s}}{m_s B}\right) + \frac{qn_s}{m_s}\langle E_\|\rangle - \left[\frac{p_{\perp_s}}{m_s} - \frac{qn_s\varphi}{m_s}\left\langle J_o\left(v_\perp^2/2v_{th}^2 - 1\right)\right\rangle\right]\frac{\partial \ln B}{\partial z},$$

where q, m_s, p_s, and $E_\|$ represent particle charge, particle mass, plasma pressure, and parallel electric field. The use of $\langle\rangle$ denotes averaging over the ion gyro-orbit. J_o is the Bessel function, and $\langle J_o(v_\perp^2/2v_{th}^2 - 1)\rangle \approx -b_i/[2(1 + b_i/2)^2]$, where $v_\perp$ and v_{th} represent the particle perpendicular and thermal velocities. For electrons, the momentum equation is closed with $p_{\perp e} = p_{\|e} = n_e T_e$, which yields

$$\frac{\partial n_e u_{\|e}}{\partial t} = -\frac{eE_\|}{m_e} - B\frac{\partial}{\partial z}\left(\frac{n_e T_e}{m_e B}\right) - \frac{n_e T_e}{m_e}\frac{\partial \ln B}{\partial z}. \tag{2}$$

The ion momentum equation is closed with $p_{\perp i} = n_i T_i$, yielding

$$\frac{\partial n_i u_{\|i}}{\partial t} = \frac{en_i E_\|}{m_i(1 + b_i/2)} - B\frac{\partial}{\partial z}\left(\frac{p_{\|i}}{m_i B}\right) - \left[\frac{n_i T_i}{m_i} - \frac{en_i\varphi}{m_i}\frac{b_i}{2(1 + b_i/2)^2}\right]\frac{\partial \ln B}{\partial z}. \tag{3}$$

The second moment of the gyrofluid equation is used to provide the ion parallel pressure:

$$\frac{\partial p_{\|i}}{\partial t} = -B\frac{\partial}{\partial z}\left(\frac{3n_i T_i u_{\|i}}{B}\right) - 2n_i T_i u_{\|i}\frac{\partial \ln B}{\partial z}. \tag{4}$$

Both perpendicular and parallel heat fluxes are assumed to be zero.

[13] The parallel electric field $E_\|$ is defined by the scalar potential ϕ and the vector potential A as

$$E_\| = -\frac{\partial A_\|}{\partial t} - \frac{\partial \varphi}{\partial z}. \tag{5}$$

The vector potential comes from Ampere's law,

$$\nabla \times \boldsymbol{B} = \nabla \times (\nabla \times \boldsymbol{A}) = \mu_o e\left(\sum_i n_i u_i - n_e u_e\right). \tag{6}$$

The scalar potential comes from the Poisson equation,

$$\nabla^2\varphi = -e/\varepsilon_o\left(\sum_i n_i - n_e\right). \tag{7}$$

The ion density, n_i, is not the same as the guiding center density, $\overline{n_i}$, but is related by $n_i = \overline{n_i} - n_{io}(1 - \Gamma_o)e\varphi/T_i$.

[14] The Lax-Wendroff method is employed to solve the above equations. The accuracy of this method is improved by applying it to half steps, which are between the grid points spatially and between time steps temporally. First, equations (1), (3), (4), and (5) are advanced in time by this method, where $A_\|$ is determined from equation (5). Equations (6) and (7) are then evaluated, where u_e is obtained from equation (6). Finally, equation (2) is evaluated to solve for $E_\|$. $E_\|$ is recorded at each time step, and $eE_\|$ acts as the electric force to advance test particles, as described in section 3.3. The order in which we solve this system of coupled equations is so chosen to include electron inertia while avoiding resolution of electron thermal velocity in the Courant condition. The detailed computational method is described by *Jones* [2004] and *Jones and Parker* [2003].

[15] The dispersion relation can be analytically solved based on equations (1)–(7) under the assumptions that the background quantities B, n_s, and T are constant. In the limit that $b_i \ll 1$, this relation reduces to the usual dispersive Alfvén wave:

$$\frac{\omega^2}{k_\|^2} \approx V_A^2\frac{1 + k_\perp^2\rho_s^2}{1 + k_\perp^2\lambda_e^2}, \tag{8}$$

where $V_A(=B/\sqrt{\sum n_i m_i \mu_o})$ is MHD Alfvén speed, $\rho_s(=\sqrt{m_i T_e/e^2B^2})$ is ion acoustic gyroradius, and $\lambda_e(=c/\omega_{pe})$ is electron skin

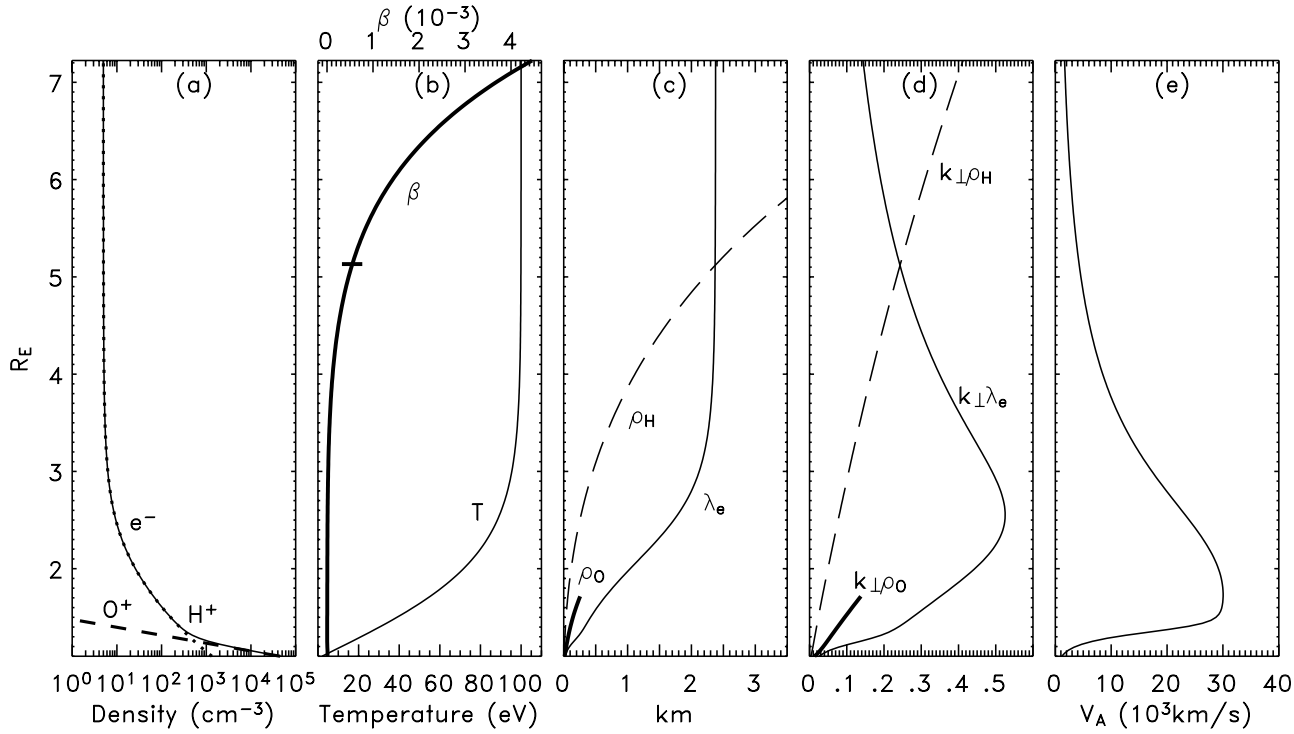

Figure 2. Initial conditions of the gyrofluid code. (a) Plasma densities, where solid, dashed, and dotted lines represent the electron, O^+, and H^+ densities. (b) The plasma temperature (thin line) and β (bold line), where the short horizontal bar indicates the location where $\beta = m_e/m_H$. (c) The electron skin depth (λ_e), H^+ gyroradius (ρ_H), and O^+ gyroradius (ρ_O) are plotted as the thin, long dashed, and bold lines, respectively. (d) $k_\perp\lambda_e$, $k_\perp\rho_H$,, are $k_\perp\rho_O$ are displayed as the thin, long dashed, and bold lines. (e) The phase speed of the dispersive Alfvén wave.

depth. The denominator of equation (8) consists of the electron inertia term, while the numerator contains the contribution of the electron pressure gradient term. When including the ion equations, a fairly complicated linear dispersion relation is obtained,

$$\sum_i \frac{n_{io}}{m_i(1+b_i/2)}\left(1-\frac{3T_i}{m_iV_P^2}\right)^{-1}+\frac{n_{eo}}{m_e}\left(1-\frac{T_e}{m_eV_P^2}\right)^{-1}+\frac{k_\perp^2}{\mu_o e^2} = \frac{k_\perp^2}{\mu_o e^2 V_P^2}\left[\frac{\sum_i \frac{n_{io}}{m_i(1+b_i/2)^2}\left(1-\frac{3T_i}{m_iV_P^2}\right)^{-1}+\frac{n_{eo}}{m_e}\left(1-\frac{T_e}{m_eV_P^2}\right)^{-1}}{\sum_i n_{io}(1-\Gamma_o)T_i^{-1}}\right], \quad (9)$$

where $V_P(=\omega/k_\parallel)$ is the phase speed of the Alfvén wave. Equation (9) is solvable as a quadratic in V_P^{-2}. A detailed derivation can be found in the work of *Jones* [2004]. A nearly perfect agreement was obtained when simulation results were compared with the valid root of analytical dispersion relations.

[16] The Landau damping effect is not considered in our model. By using the local, homogeneous dispersion relation, *Lysak and Lotko* [1996] found that the Landau damping rate is less than ~0.1 of the wave frequency whenever the wave number satisfied both $k_\perp\rho_s < 1$ and $k_\perp\lambda_e < 1$. Moreover, their results indicate that low-frequency Alfvén waves with perpendicular wavelengths greater than the order of 10 km when mapped to the ionosphere will not be significantly affected by Landau damping. On the basis of the initial parameters chosen for our simulations, Landau damping should not play a significant role. We should point out, however, that the effect of Landau damping in an inhomogeneous environment, such as our model, has not been fully investigated. This problem is to be the subject of future studies.

3.2. Initial Conditions and Background Parameters

[17] The background parameters for the gyrofluid code are shown in Figure 2. The lower (ionospheric) and upper (magnetospheric) boundaries are chosen at 1.1 and 7.2 R_E geocentric distance. Density profiles are displayed in Figure 2a, where the dashed, dotted, and solid lines represent H^+, O^+, and e^- densities, respectively. In order to obtain the density profile, 330 orbits were collected by the FAST satellite as it passed through the dayside auroral region. The spin-averaged plasma densities were estimated by Langmuir probes. It should be noted that there are uncertainties at low altitudes due to an unknown electron temperature; however, our estimations of the plasma density between 2000 and 4500 km (in the acceleration regions) are believed to be accurate. For convenience, mathematical equations were used to fit the median values of plasma densities. The density profile (solid line) in Figures 2a has the form $n_O(r) = 5 \times 10^5 \exp((1.0157 - r)/0.035)$ for O^+ (dashed line), where n_O is in cm^{-3} and r is in R_E, and $n_H = n_M + n_I$ with $n_M(r) = 2600/r^7$ and $n_I(r) = 17.684 \tanh(1.808 \times r - 0.337) - 12.7$ for H^+ (dotted

line), where n_M and n_I are the magnetosheath and ionospheric contributions, respectively. It should be noted that we modified the O^+ and H^+ density profiles in order to obtain the electron burst signature (see detailed description in section 4.2).

[18] The bold line in Figure 2b represents $\beta(=\mu_o nT/B^2)$. The short horizontal bar at $\sim$5.1 R_E indicates where $\beta = m_e/m_H$. The temperatures of the upper (magnetosheath) and lower (ionosphere) boundaries are assumed to be 100 and 2 eV, respectively. The thin line in Figure 2b represents temperatures with a form $T = 2 + 98\tanh(r - 1.0157)$. On the basis of models of the dispersive field line resonances, *Streltsov et al.* [1998] and *Rankin et al.* [1999] indicated that the parallel electric field decreases with increasing ion and electron temperature ratio. This effect is not significant in the auroral acceleration region where the electron inertia is dominant. In this paper we simply assume the ion temperature to be the same as the electron temperature. If we had wished to consider hot magnetosheath ions ($T_i > T_e$), it may have been necessary to increase the initial perturbation at high altitudes in order to obtain the same magnitude of the parallel electric field in the acceleration region. Because the selection of the initial pulse was based on amplitudes observed at low altitudes, the effect of $T_i > T_e$ is not relevant to this study.

[19] From FAST observations at 1500–2300 km altitudes in the dayside auroral regions, *Chaston et al.* [1999] showed an averaged value of the perpendicular scale sizes of Alfvén waves to be 590 m. It is believed that auroral forms and vortex structures with scale sizes of 0.1–10 km (referenced to the ionospheric height) are related to the nonlinear Alfvén wave phenomena [*Stasiewicz et al.*, 2000, and references therein]. In our study, the perpendicular wave number ($k_\perp$) is assumed to be $\sim$1 km^{-1} (i.e., a perpendicular wavelength of 6.3 km) at the ionospheric boundary and is inversely proportional to the radius of the magnetic flux tube (i.e., $k_\perp \propto B^{1/2}$ for a dipole field).

[20] The electron skin depth (λ_e), H^+ gyroradius (ρ_H), and O^+ gyroradius (ρ_O) are plotted in Figure 2c, while $k_\perp\lambda_e$, $k_\perp\rho_H$, and $k_\perp\rho_O$ are displayed in Figure 2d. The kinetic Alfvén wave ($k_\perp\rho_H > k_\perp\lambda_e$) appears in an intermediate beta plasma with $m_e/m_H < \beta < 1$ at altitudes above 5.1 R_E, while the inertial Alfvén wave ($k_\perp\rho_H < k_\perp\lambda_e$) arises in a low-beta plasma with $\beta < m_e/m_H$ at altitudes below 5.1 R_E. The phase velocity of the dispersive Alfvén wave is plotted in Figure 2e, where the peak is located at $\sim$1.6 R_E.

[21] As suggested by *Lysak* [1991, 1993] and *Chaston et al.* [2002a], the ionospheric Alfvén resonator may modify the Alfvén wave propagation. Although the gyrofluid code is also capable of studying the ionospheric Alfvén resonator, such investigation is beyond the scope of this paper. Here, we assume the ionosphere is a perfect conducting boundary and focus on the effect in the acceleration region before the wave reaches the ionospheric boundary.

[22] The simulation is initialized with an electron density perturbation of a single Gaussian pulse near the upper boundary of the flux tube and then allowed to evolve in time. The parallel wavelength of this initial pulse is $\sim$0.13 R_E. The physical mechanism responsible for the generation of the field perturbation is not addressed here. It may, for example, come from low-frequency hydromagnetic waves excited from a region where reconnection is occurring at the dayside magnetopause. Various magnitudes of initial density perturbations were tested to create an assortment of parallel electric fields. Our results were compared most favorably with the FAST data when the parallel electric field has a magnitude of $\sim$0.2 mV/m at the acceleration region.

3.3. Test Particle Method

[23] Our primary focus is to study kinetic electron distributions by tracking a distribution of test particles in the simulation and following their evolution with Alfvén waves. Kinetic equations for the electrons in the direction parallel to the magnetic field are described as below:

$$\frac{\partial x_\parallel}{\partial t} = v_\parallel \hat{b}, \tag{10}$$

$$m_e \frac{\partial v_\parallel}{\partial t} = -eE_\parallel - \mu\left(\hat{b}\cdot\nabla \boldsymbol{B}\right), \tag{11}$$

where $\hat{b}$ is the direction along the magnetic field line and $\mu = m_e v_\perp^2/(2B)$. The gravitational force is neglected for electrons. $E_\parallel$ is evolved in the gyrofluid code as a function of time and position along the magnetic field line. It should be noted that the test particle approach is not self-consistent. Particles evolve due to the wave field, but their dynamics do not couple back to the gyrofluid model describing the waves.

[24] A Maxwellian electron distribution function with a temperature of 100 eV is introduced from the top of the field line (i.e., the magnetopause boundary) to represent precipitating magnetosheath electrons. Electrons outside the loss cone will be reflected due to the mirror force. Cold ($\sim$2 eV) ionospheric electrons are also introduced as the background population along the flux tube. We allow particles to fill the flux tube and reach a steady state before launching an Alfvén wave. There are approximately 300,000 and 376,000 test particles to represent magnetosheath and background electrons, respectively, in the entire flux tube. Fresh particles are injected from both upper and lower boundaries at each time step. The position, parallel and perpendicular velocities, and phase space density of each particle are recorded at each time step until the particle escapes from the simulated flux tube.

4. Simulation Results

4.1. Time Dispersive Signature

[25] Although several previous studies have successfully reproduced electron time dispersive signatures [*Kletzing and Hu*, 2001; *Andersson et al.*, 2002], it is important to verify these results for the dayside and validate our model. Figures 3a–3d show the snapshots of test particles and the parallel electric field at time 0.8, 1.5, 2.0, and 2.11 s. The parallel velocities and positions of background cold electrons and magnetosheath electrons are plotted in the left and right panels, respectively. The thin and bold solid lines in the middle panel represent the phase speed of the Alfvén wave and the parallel electric field, respectively, obtained from the gyrofluid code. The parallel wavelength and the magnitude of the parallel electric field increase

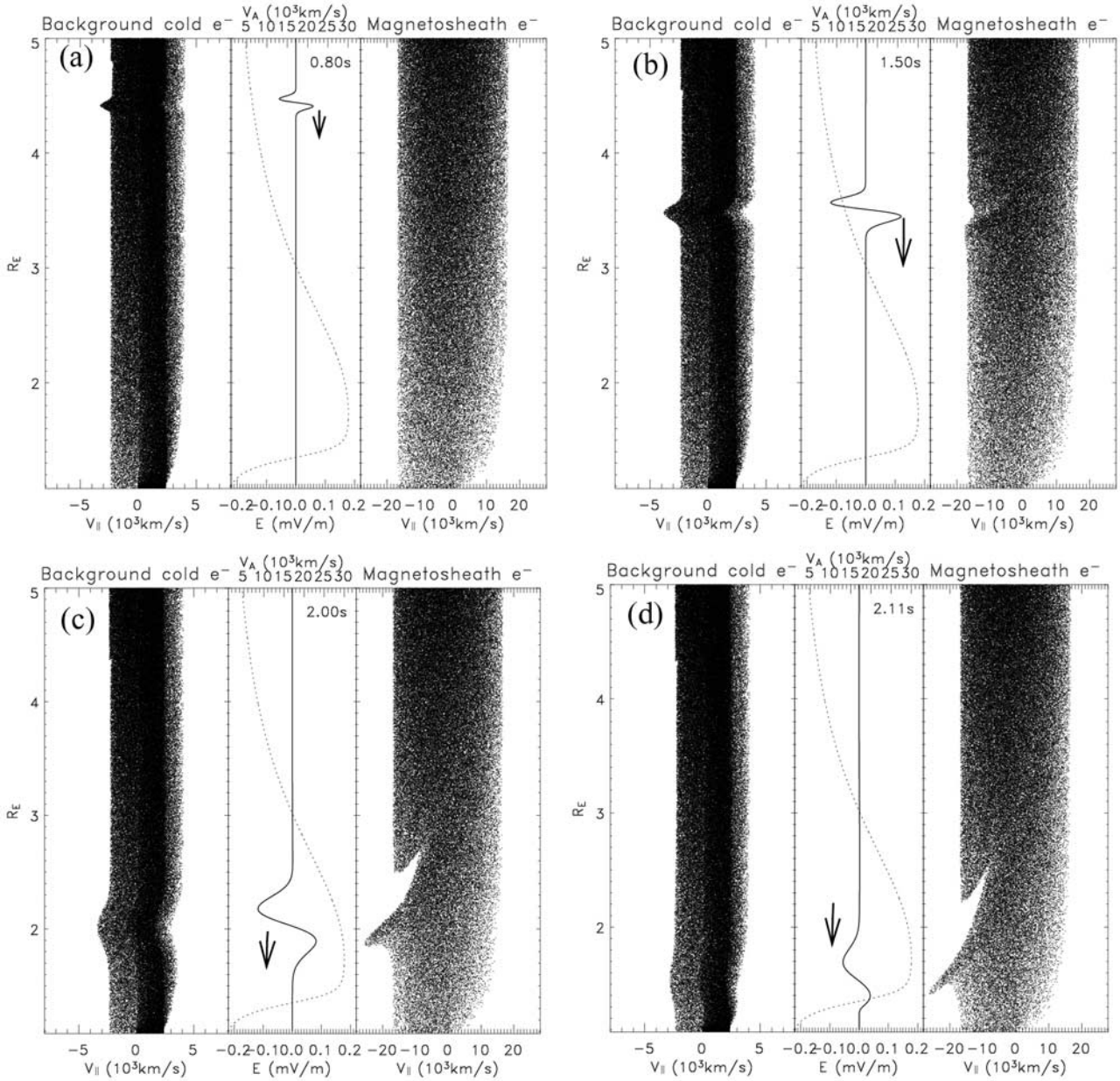

Figure 3. Four snapshots of parallel velocities of cold electrons (left), parallel electric fields and Alfvén speeds (middle), and parallel velocities of magnetosheath electrons (right) along the flux tubes at times (a) 0.8, (b) 1.5, (c) 2.0, and (d) 2.11 s.

with increasing wave speed above the peak of the Alfvén speed (Figures 3a–3c). Once below the peak (Figure 3d), the amplitude of the parallel electric field decreases substantially because the density rises very quickly at low altitudes and the electron skin depth becomes small.

[26] In the kinetic regime the parallel electric field appears to have the same phase as the gradient of the scalar potential (not shown here), while it has the opposite phase in the inertial regime. The parallel electric field is nearly reduced to zero at 5.1 R_E, a transition region from the kinetic to the inertial regime. The altitude of the transition region decreases with increasing magnetosheath density. The behavior of the parallel electric field near the transition region can be explained by equation (12) assuming $b_i \ll 1$. On the basis of equations (5), (6), (1), (7), and (8), the parallel electric field can be written as

$$E_\parallel = -ik_\parallel\phi\left(1-\frac{\omega^2}{k_\parallel^2}V_A^{-2}\right) \approx -ik_\parallel\phi\left(\frac{k_\perp^2\lambda_e^2-k_\perp^2\rho_s^2}{1+k_\perp^2\lambda_e^2}\right). \quad (12)$$

The parallel electric field behavior is also consistent with the results based on equation (14) from *Streltsov and Lotko* [1998].

[27] In earlier results, electron distributions are not modified significantly from the initial Maxwellian distribution due to a small parallel electric field in the kinetic region. Hence the time zero of our test particle procedure in this

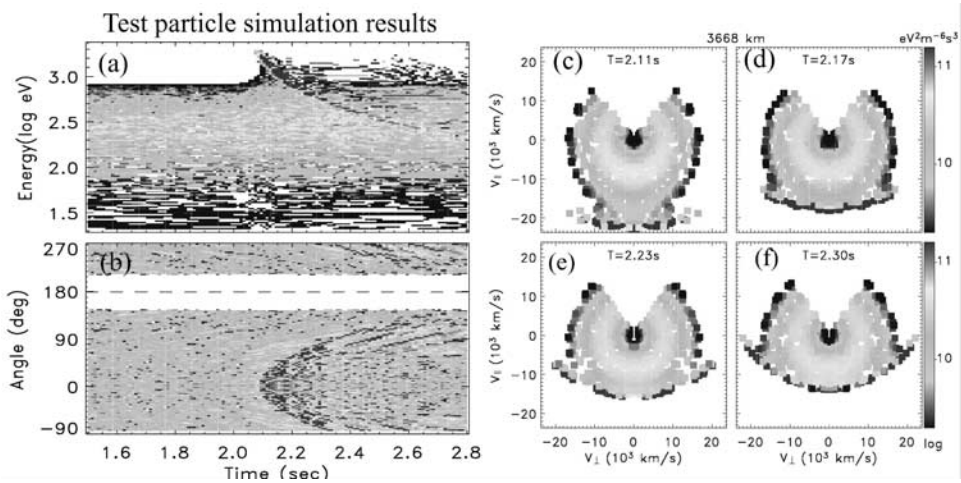

Figure 4. (a) Energy-time and (b) angular-time spectrograms of magnetosheath electrons at 3668 km altitude, where 0° (180°) indicates the direction parallel (antiparallel) to the local magnetic field. Distribution functions of magnetosheath electrons at (c) 2.11, (d) 2.17, (e) 2.23, and (f) 2.30 s. See color version of this figure at back of this issue.

article is set when the wave propagates through the transition region. Although we filled the flux tube with test particles up to ~7.2 R_E, Figure 4 presents particles between the ionospheric boundary and ~5 R_E.

[28] In this simulation, the cold background electrons are not substantially accelerated by the Alfvén wave (the acceleration of background electrons is discussed in section 4.2 with different initial density profiles). The strongest acceleration is in the warm magnetosheath electrons (the right panel in Figures 3c–3d). Electrons are accelerated downward toward the ionosphere due to a positive (antiearthward) parallel electric field at the leading edge of the wave. Particles with higher energies move faster than ones with lower energies along the flux tube, which create the energy-time dispersion at a fixed location as shown in Figure 4a. Figures 4a and 4b present the energy and pitch angle spectrograms of magnetosheath electrons at 3668 km altitude, where 0° (180°) is the direction downward (upward) to the ionosphere. Snapshots of magnetosheath electron distribution functions are plotted in Figures 4c–4f. The highest-energy electrons first appear at small pitch angles and evolve to larger pitch angles with time from a bow shape structure in the angular spectrogram (Figure 4b). The simulation results in Figure 4 resemble the FAST observation from 0833:26.5 to 0833:27 UT in Figure 1 with the exception of the low-energy burst signature. The time span (~0.5 s) and the energy of the dispersive signature from our simulation results are comparable to those from the observation.

[29] A reversed phase of the initial density perturbation was also studied (results not shown here), where a negative parallel electric field was created in the leading edge of the wave below the transition region while a positive field was generated in the trailing edge. The dispersion signature was still present; however, the energy dispersion developed at the trailing edge of the wave as opposed to the leading edge as was shown in Figure 3.

4.2. Electron Burst Signature

[30] Low-energy electron bursts are the most frequently observed signatures in the auroral oval, particularly in the dayside region; even so, they are the least studied signatures by modelers. It is believed that cold electrons are trapped within the wave and gain energy as the Alfvén wave propagates down toward the ionosphere [*Andersson et al.*, 2002]. Electron bursts are often observed together with the electric and magnetic field perturbations, where the $E_\perp/B_\perp$ ratio is on the same order of the local Alfvén speed [*Chaston et al.*, 1999]. Additionally, *Su et al.* [2001] showed the energy flux of electron bursts to be well correlated with the perpendicular electric field of Alfvén waves. The most important finding of this study is the determination of the appropriate background parameters to produce field-aligned electron bursts.

[31] In the simulation described in section 4.1, the cold electrons were not substantially trapped by the wave. Particle trapping requires a parallel electric field of significantly larger amplitude and/or a substantially slower wave phase speed (the phase speed should be comparable to the electron thermal speed). It should be noted that the electron trapping described in this paper is different from that shown in the phase space diagram discussed by *Clark and Seyler* [1999]. Rather, the trapping referred to in this paper is similar to the Fermi-like resonance described by *Kletzing* [1994], which differs from the ionospheric resonator [*Lysak*, 1991, 1993]. In a pure H^+ plasma the amplitude of the parallel electric field decreases as the wave phase speed decreases with increasing electron density. The wave amplitude ($E_\parallel$, $E_\perp$) would have to be increased to a level well beyond that consistent with observations at FAST altitudes to allow cold electrons to be resonant with the wave. The presence of O^+, however, may cause the Alfvén wave speed to decrease without significantly lowering the parallel electric field (i.e., the total electron density remains the same). This hypothesis of increasing the mass density without modifying the electron density is tested by the simulation presented below.

[32] The initial conditions shown in Figure 5 are modified from those in Figure 2 to determine whether wave trapping could occur, which could result in a cold electron burst. The temperature profile in Figure 5b is the same as that in

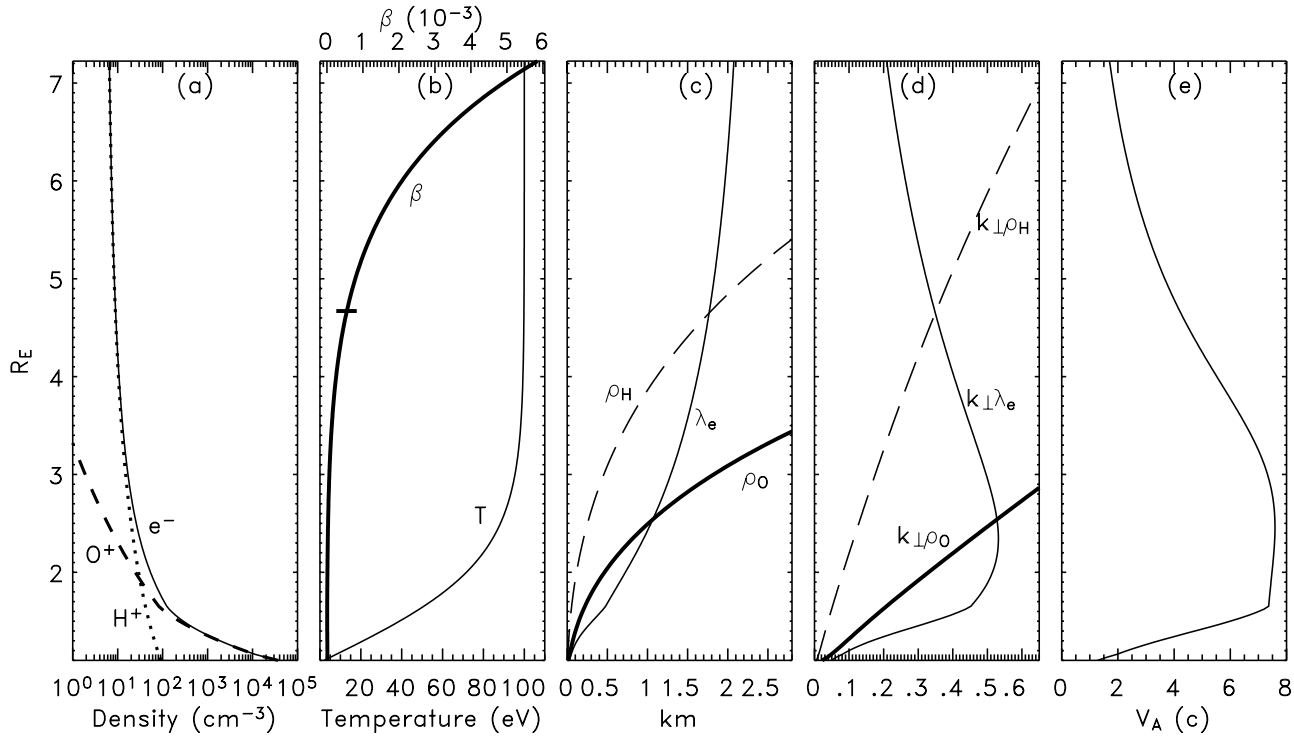

Figure 5. Initial condition of the gyrofluid code for generating an electron burst signature. The format is the same as that shown in Figure 2.

Figure 2b. Although the total density is similar to that in Figure 2a, the composition of O^+ and H^+ differs below ~3 R_E, which results in a different wave speed profile in Figure 5e than in Figure 2e. An increase in O^+ density results in a decrease of the wave speed. The peak of the Alfvén speed is located at ~2.7 R_E, and the Alfvén speed only decreases slightly from 2.7 to 1.6 R_E before the total density rises dramatically with decreasing altitudes causing the parallel electric field to vanish. The kinetic effect is dominant above 4.7 R_E where $k_\perp \rho_H > k_\perp \lambda_e$. Owing to an increase in O^+ density below 3 R_E, the O^+ gyroradius effect decreases the phase speed of the wave while the two-fluid MHD model yield the opposite effect.

[33] The position versus parallel velocities of background electrons are plotted in the left panel of each plot in Figure 6, while the wave speed (thin line) and the parallel electric field (bold line) are on the right. In this run, a slower wave velocity causes cold background electrons to resonant with the wave and gain energy as it propagates downward. At regions between 2.7 and 1.6 R_E, the parallel wavelength is slightly shortened and the parallel electric field still remains at a substantial enough magnitude to accelerate electrons trapped within the wave. The highest parallel velocity of electrons reaches 14×10^3 km s^{-1}, twice the local Alfvén speed.

[34] The perpendicular electric and magnetic fields along with energy and pitch angle spectrograms of background electrons at an altitude of 4476 km are presented in Figures 7a–7d. The altitude selected here is to best present our result although it is slightly higher than the apogee of the FAST satellite. With slightly changes in the density profile, the acceleration region can be shifted higher or lower in altitudes.

[35] Although the peaks of the perpendicular electric and magnetic fields in Figure 7a–7b are approximately twice the magnitude of the observed fields shown in Figure 1a–1b, they are comparable to other observations in the dayside auroral region [e.g., *Andersson et al.*, 2002]. A few electrons at the highest energy level travel in front of the wave, while most accelerated electrons move together with the wave generating a burst signature as seen in Figure 7c. These electrons are present within narrow pitch angles (−40° to 40°) in the downward direction and wide energy ranges from ~10 to 250 eV. Four snapshots of distribution functions of background electrons at 4476 km are shown in Figures 7e–7h. In Figure 7e, an original cold electron distribution function is presented prior to the wave reaching the altitude of 4476 km. Accelerated electron distributions, with the wave passing through this region, are shown in Figures 7f–7h. The spectrograms (Figures 7c–7d) obtained from the simulation are comparable to the observed burst signatures in Figures 1c–1d.

[36] When we reversed the phase of the initial density perturbation (i.e., reversing the phase of the parallel electric field), the resonant electrons were found to be in the upward direction rather than the downward direction as shown in Figure 6. No substantial electron acceleration was observed due to this change in the initial perturbation.

5. Discussions and Conclusion

[37] In this study, a linear 1-D gyrofluid code is adopted to determine propagation characteristics of dispersive Alfvén waves in an inhomogeneous M-I coupling region. This model includes the electron inertial, electron pressure gradient, and finite ion gyroradius effects. Although the

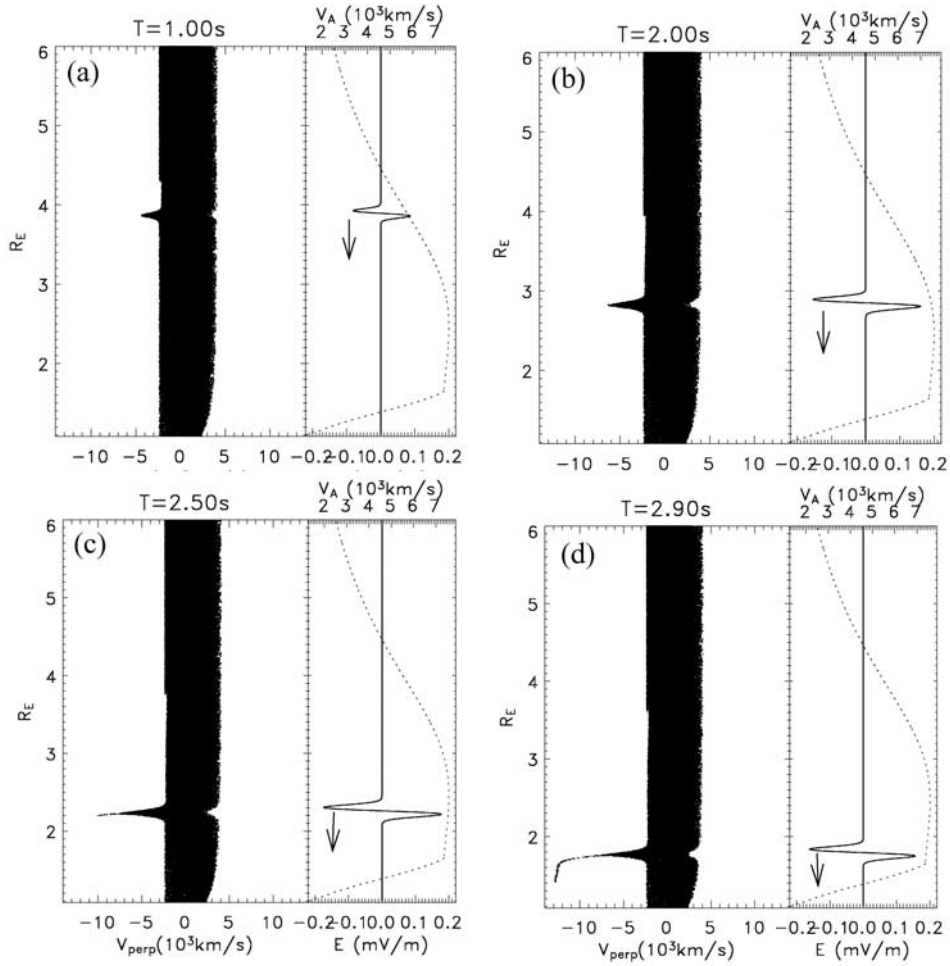

Figure 6. Four snapshots of parallel velocities of cold electrons (left) and parallel electric fields and Alfvén speeds (right) along the flux tubes at times (a) 1.0, (b) 2.0, (c) 2.5, and (d) 2.9 s.

perpendicular wave number is an input parameter of the gyrofluid code, we can validate $k_\perp$ by comparing simulated perpendicular electric fields with in situ observations. In order to obtain the comparable observed perpendicular electric fields of hundreds of mV m^{-1}, $k_\perp$ should be on the order of 1 km^{-1} at the ionospheric boundary. Although the test particle approach is not a self-consistent study, it does allow for a close examination of electron distributions under the influence of dispersive Alfvén waves.

[38] By using a 1-D gyrofluid code with a test particle method, we have successfully reproduced not only the energy and pitch-angle dispersion but also field-aligned electron bursts observed by the FAST satellite in the dayside auroral region. The time span of the dispersion signature from our simulation, approximately 0.5 s, is comparable to that of the observation. The time dispersion is generated by precipitating magnetosheath electrons due to a propagating Alfvén wave where the electron inertia is the dominant effect at the acceleration region. The time dispersion signature of the plasma sheet electrons has also been modeled by *Kletzing and Hu* [2001] due to the variation in the Alfvén speed. Our results show that higher-energy electrons arrive to a fixed location (about FAST apogee) earlier than lower-energy ones. Additionally, electrons with the highest energy level first appear at small pitch angles, evolving to larger pitch angles with time. We are able to explain the pitch angle structure of the dispersion due to the inclusion of the mirror force. *Thompson and Lysak* [1996] were the first to include a dipole magnetic field in their electron acceleration study. *Chaston et al.* [2000] and *Andersson et al.* [2002] have also demonstrated similar pitch angle dispersions in their studies.

[39] Field-aligned electron bursts with energies of tens to hundreds eV are the most commonly observed signatures in the dayside auroral region. *Clark and Seyler* [1999] showed that cold electrons can be energized to a few hundreds times the electron thermal energy by a nonlinear wave evolution. *Chaston et al.* [2000] have shown that the propagating inertial Alfvén wave is able to generate field-aligned electrons with a broad energy spread reaching a maximum energy of ~600 eV. The energy obtained from their test particles is higher than that of the observation. Moreover, O^+ ions were not taken into account in their model. In this paper, we have demonstrated that field-aligned superthermal electrons can be generated by a linear dispersive Alfvén wave in an O^+ dominant flux tube but do not exclude other mechanisms.

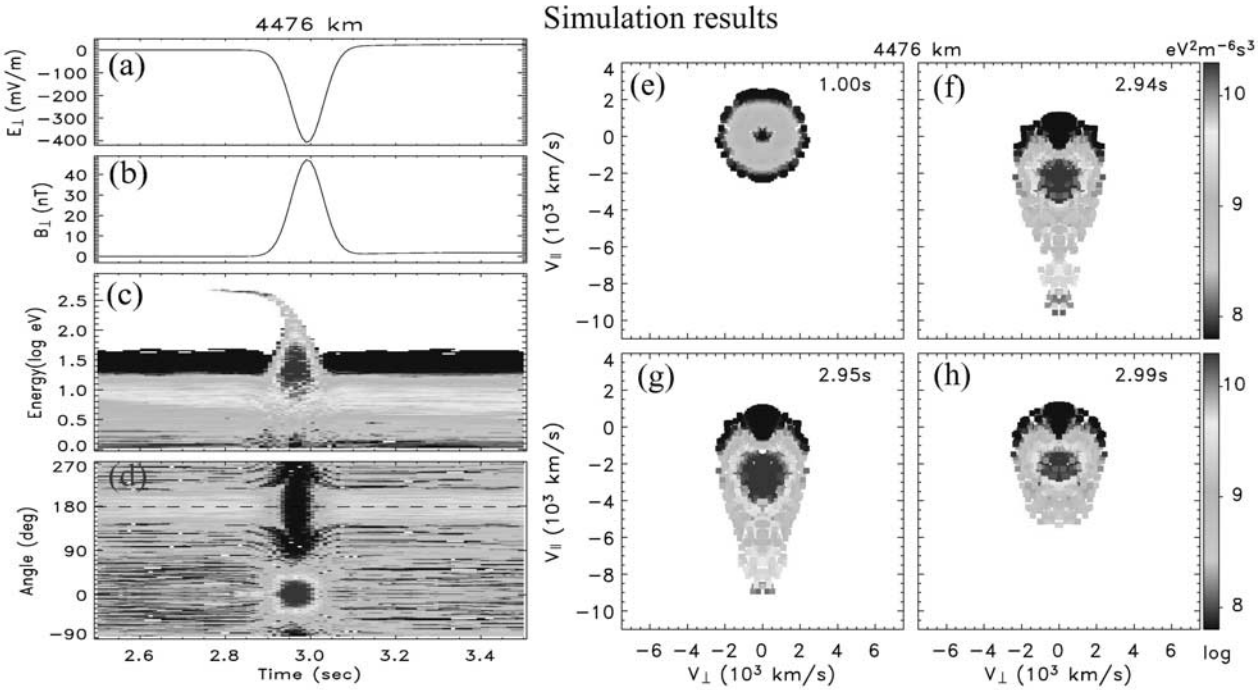

Figure 7. (a) Perpendicular electric and (b) magnetic fields and (c) energy-time and (d) (d) angular-time spectrograms of background electrons at 4476 km altitude. Distribution functions of magnetosheath electrons at times (e) 1.00, (f) 2.94, (g) 2.95, and (h) 2.99 s. See color version of this figure at back of this issue.

[40] From this study, we learn that the phase speed of the Alfvén wave plays a critical role in generating suitable conditions for the formation of the cold electron burst signature. The Alfvén speed is closely related with the local mass density. Precise density measurements are essential in understanding Alfvén wave properties and electron acceleration.

[41] Particle resonance requires the phase speed of the Alfvén wave to be comparable to the electron thermal speed. In order to produce cold electron trapping, the mass density was increased (i.e., increasing O^+ density) to reduce the Alfvén speed to ~4 times lower than that used in the dispersive case. Furthermore, a region of gradually ramping Alfvén speed in the acceleration region maintains accelerated electrons trapped within the wave to low altitudes. Here, the comparison between the ideal Alfvén speed (dotted line), the Alfvén speed with inertial correction (dashed line), Alfvén speed with electron inertial and pressure corrections (long dashed line), and the phase speed of the Alfvén wave derived from equation (9) (solid line) is shown in Figure 8 based on the same density profile (Figure 5a). For the electron burst case the acceleration region is located between the peak of the Alfvén speed (~2.7 R_E) and the drop-off of the wave speed (1.6 R_E). In this region the parallel wavelength and the wave speed slightly decrease with decreasing altitudes, while the parallel electric field continues to be maintained at a magnitude substantial enough (~0.2 mV m^{-1}) to accelerate background cold electrons. The phase speed of the Alfvén wave is highly dependent on the density and the composition of the plasma. Although the total densities are similar for both dispersion and burst cases, O^+ (H^+) densities are increased (decreased) below 3 R_E in the burst case (section 4.2). Previous studies [*Kletzing*, 1994; *Kletzing and Hu*, 2001; *Chaston et al.*, 2000, 2002a, 2002b] only considered the inertial effect near the acceleration region. *Chaston et al.* [2003] showed that the kinetic effect acts to increase the wave speed opposite of the electron inertial effect. Although

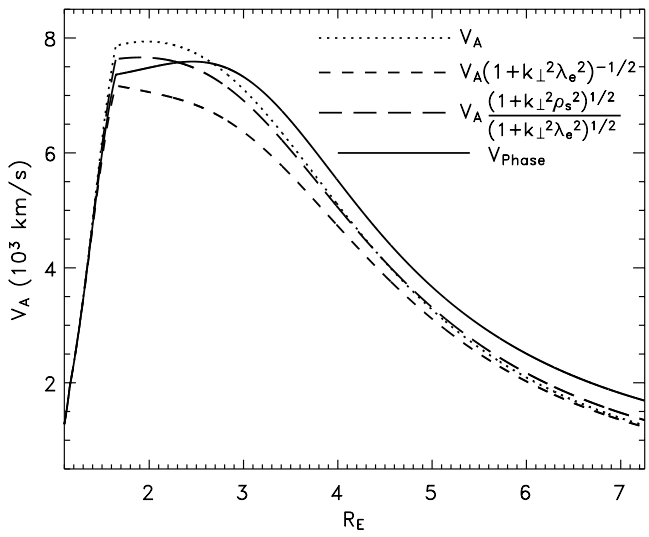

Figure 8. Comparison of three Alfvén velocities, where the dotted, dashed, long-dashed, and solid lines represent the MHD Alfvén speed, inertial Alfvén speed, Alfvén speed with electron inertial and pressure corrections, and the phase speed of the Alfvén wave from the gyrofluid code, respectively, based on the same density profile shown in Figure 5a.

electron inertia is the primary effect at low altitudes, the full gyrokinetic effect plays a role in altering the shape of the phase speed profile and maintaining electron acceleration to low altitudes. From our investigation, we learn that it is important to include O^+ ions to study the acceleration process of cold electrons. O^+ densities have been included in previous studies [e.g., *Kletzing and Hu*, 2001; *Thompson and Lysak*, 1996; *Chaston et al.*, 2003]; however, the scale height of O^+ ions used in this paper is greater than that used in previous nightside auroral studies. The greater O^+ scale height in the dayside/cusp region may be the reason why the superthermal electron bursts are more commonly observed in the dayside

[42] The particle signature shows that few electrons are accelerated by the wave potential with sufficient energy to travel in front of the wave. These electrons reach a parallel speed of a factor of two times of the Alfvén speed as reported by *Kletzing* [1994]. The majority of the electrons are trapped within the wave and gain energy in the field-aligned direction by the parallel electric field. In order for the test particle results to be meaningful the energy flux in the accelerated electron distributions must be less than or equal to the wave Poynting flux. For the electron burst case, the Poynting flux at 4476 km altitude is approximately 14.3 erg s^{-1} cm^{-2}, where perpendicular electric and magnetic field perturbations are $\sim$400 mV m^{-1} and $\sim$45 nT, respectively. An integrated energy flux of accelerated electrons is estimated to be 2.88 erg s^{-1} cm^{-2} or $\sim$20% of the Alfvén wave Poynting flux.

[43] The simulation presented in this paper is initialized by a single pulse perturbation generating an electron burst signature with a time period of $\sim$0.1 s. The continuous electron bursts from observations may be due to multiple pulse perturbations (temporal effect), the satellite passing through different flux tubes (spatial effect), or a combination of the two.

[44] Observations of electric fields within Alfvén waves from satellite and rocket data indicate that the fields are of multiple scales and are rarely periodic. Electric field amplitudes at smaller scales may be greater than those at larger scales possibly due to the inertial correction, which may cause spikes in phase space and disturb the trapped electron orbits. In this paper, we simply present resonant electrons due to a coherent waveform. Wave trapping by more realistic disturbances is a topic for future studies.

[45] **Acknowledgments.** The authors would like to thank Laila Andersson, Chris Chaston, and Bob Lysak for helpful discussions. This research was supported by NASA grants NAG5-11924, NAG5-12026, NAG5-3596, and NAG5-12590 and NSF grant ATM-0202564 to the University of Colorado.

[46] Arthur Richmond thanks the reviewers for their assistance in evaluating this paper.

References

Andersson, L., N. Ivchenko, J. Clemmons, A. A. Namgaladze, B. Gustavsson, J.-E. Wahlund, L. Eliasson, and R. Y. Yurik (2002), Electron signatures and Alfvén waves, *J. Geophys. Res.*, *107*(A9), 1244, doi:10.1029/2001JA900096.

André, M., and L. Eliasson (1995), Some electron conic generation mechanisms, in *Space Plasma: Coupling Between Small and Medium Scale Processes*, *Geophys. Monogr. Ser.*, vol. 86, edited by M. Ashour-Abdalla, T. Chang, and P. Dusenbery, p. 61, AGU, Washington, D.C.

Beer, M. A., and G. W. Hammett (1996), Toroidal gyrofluid equations for simulations of tokamak turbulence, *Phys. Plasma*, *3*, 4046.

Chaston, C. C., C. W. Carlson, W. J. Peria, R. E. Ergun, and J. P. McFadden (1999), FAST observations of inertial Alfvén waves in the dayside aurora, *Geophys. Res. Lett.*, *26*, 647.

Chaston, C. C., C. W. Carlson, R. E. Ergun, and J. P. McFadden (2000), Alfvén waves, density cavities and electron acceleration observed from the FAST spacecraft, *Phys. Scr.*, *T84*, 64.

Chaston, C. C., J. W. Bonnell, C. W. Carlson, M. Berthomier, L. M. Peticolas, I. Roth, J. P. McFadden, R. E. Ergun, and R. J. Strangeway (2002a), Electron acceleration in the ionospheric Alfvén resonator, *J. Geophys. Res.*, *107*(A11), 1413, doi:10.1029/2002JA009272.

Chaston, C. C., J. W. Bonnell, L. M. Peticolas, C. W. Carlson, J. P. McFadden, and R. E. Ergun (2002b), Driven Alfvén waves and electron acceleration: A FAST case study, *Geophys. Res. Lett.*, *29*(11), 1535, doi:10.1029/2001GL013842.

Chaston, C. C., J. W. Bonnell, C. W. Carlson, J. P. McFadden, R. J. Strangeway, and R. E. Ergun (2003), Kinetic effects in the acceleration of auroral electrons in small scale Alfvén waves: A FAST case study, *Geophys. Res. Lett.*, *30*(6), 1289, doi:10.1029/2002GL015777.

Clark, A. E., and C. E. Seyler (1999), Electron beam formation by small-scale oblique inertial Alfvén waves, *J. Geophys. Res.*, *104*, 17,233.

Clemmons, J. H., C. W. Carlson, and M. H. Boehm (1995), Impulsive ion injections in the morning auroral region, *J. Geophys. Res.*, *100*, 12,133.

Génot, V., P. Louarn, and F. Mottez (2001), Fast evolving spatial structure of auroral parallel electric fields, *J. Geophys. Res.*, *106*, 29,633.

Goertz, C. K., and R. W. Boswell (1979), Magnetosphere-ionosphere coupling, *J. Geophys. Res.*, *84*, 7239.

Hasegawa, A. (1976), Particle acceleration by MHD surface wave and formation of aurora, *J. Geophys. Res.*, *81*, 5083.

Hoffman, R. A., and D. S. Evans (1968), Field-aligned electron bursts at high latitude observation by Ogo 4, *J. Geophys. Res.*, *73*, 6201.

Hui, C.-H., and C. E. Seyler (1992), Electron acceleration by Alfvén waves in the magnetosphere, *J. Geophys. Res.*, *97*, 3953.

Johnstone, A. D., and J. D. Winningham (1982), Satellite observation of suprathermal electron bursts, *Geophys. Res. Let.*, *87*, 2321.

Jones, S. T. (2004), Gyrofluid simulation of Alfvén waves in the magnetosphere and ionosphere, Ph.D. dissertation, Dep. of Phys., Univ. of Colo., Boulder, Colo.

Jones, S. T., and S. E. Parker (2003), Including electron inertia without advancing electron flow, *J. Comput. Phys.*, *191*, 322.

Kletzing, C. A. (1994), Electron acceleration by kinetic Alfvén waves, *J. Geophys. Res.*, *99*, 11,095.

Kletzing, C. A., and S. Hu (2001), Alfvén wave generated electron time dispersion, *Geophys. Res. Lett.*, *28*, 693.

Knudsen, D. J. (1996), Spatial modulation of electron energy and density by nonlinear stationary inertial Alfvén waves, *J. Geophys. Res.*, *101*, 10,761.

Lu, J. Y., R. Rankin, R. Marchand, V. T. Tikhonchuk, and J. Wanliss (1996), Finite element modeling of nonlinear dispersive field line resonances: Trapped shear Alfvén waves inside field-aligned density structures, *J. Geophys. Res.*, *108*(A11), 1394, doi:10.1029/2003JA010035.

Lysak, R. L. (1991), Feedback instability of the ionospheric resonant cavity, *J. Geophys. Res.*, *96*, 1553.

Lysak, R. L. (1993), Generalized model of the ionospheric Alfvén resonator, in *Auroral Plasma Dynamics*, *Geophys. Monogr. Ser.*, vol. 80, edited by R. L. Lysak, pp. 121–128, AGU, Washington, D. C.

Lysak, R. L., and W. Lotko (1996), On the kinetic dispersion relation for shear Alfvén waves, *J. Geophys. Res.*, *101*, 5085.

Marklund, G. T., L. G. Blomberg, C.-G. Fälthammar, R. E. Erlandson, and T. A. Potemra (1990), Signatures of the high-altitude polar cusp and dayside auroral regions as seen by the Viking electric field experiment, *J. Geophys. Res.*, *95*, 5767.

Matsuoka, A., K. Tsuruda, H. Hayakawa, T. Mukai, A. Nishida, T. Okada, N. Kaya, and H. Fukunishi (1993), Electric field fluctuations and charged particle precipitation in the cusp, *J. Geophys. Res.*, *98*, 11,225.

McFadden, J. P., C. W. Carlson, and M. H. Boehm (1986), Field-aligned electron precipitation at the edge of an arc, *J. Geophys. Res.*, *91*, 1723.

Nakamura, T., and T. Tamao (1989), On propagation mechanisms of localized field-aligned currents in the magnetosphere, *J. Geophys. Res.*, *94*, 114.

Pfaff, R., et al. (1998), Initial FAST observations of acceleration processes in the cusp, *Geophys. Res. Lett.*, *25*, 2037.

Rankin, R., J. C. Samson, V. T. Tikhonchuk, and I. Voronkov (1999), Auroral density fluctuations on dispersive field line resonances, *J. Geophys. Res.*, *104*, 4399.

Seyler, C. E., A. E. Clark, J. Bonnell, and J.-E. Wahlund (1998), Electrostatic broadband ELF wave emission by Alfvén wave breaking, *J. Geophys. Res.*, *103*, 7027.

Stasiewicz, K., et al. (2000), Small scale Alfvénic structure in the aurora, *Space Sci. Rev.*, *92*, 423.

Streltsov, A., and W. Lotko (1995), Dispersive field line resonances on auroral field lines, *J. Geophys. Res.*, *100*, 19,457.

Streltsov, A. V., W. Lotko, J. R. Johnson, and C. Z. Cheng (1998), Small-scale, dispersive field line resonances in the hot magnetospheric plasma, *J. Geophys. Res.*, *103*, 26,559.

Su, Y.-J., R. E. Ergun, W. K. Peterson, T. G. Onsager, R. Pfaff, C. W. Carlson, and R. J. Strangeway (2001), Fast Auroral Snapshot observations of cusp electron and ion structures, *J. Geophys. Res.*, *106*, 25,595.

Thompson, B. J., and R. L. Lysak (1996), Electron acceleration by inertial Alfvén waves, *J. Geophys. Res.*, *101*, 5359.

R. E. Ergun and Y.-J. Su, Laboratory for Atmospheric and Space Physics, University of Colorado, Boulder, CO 80303, USA. (ree@fast.colorado.edu; ysu@lasp.colorado.edu)

S. T. Jones and S. E. Parker, Center for Integrated Plasma Studies, University of Colorado, Boulder, CO 80309, USA. (ssjones@colorado.edu; sparker@colorado.edu)

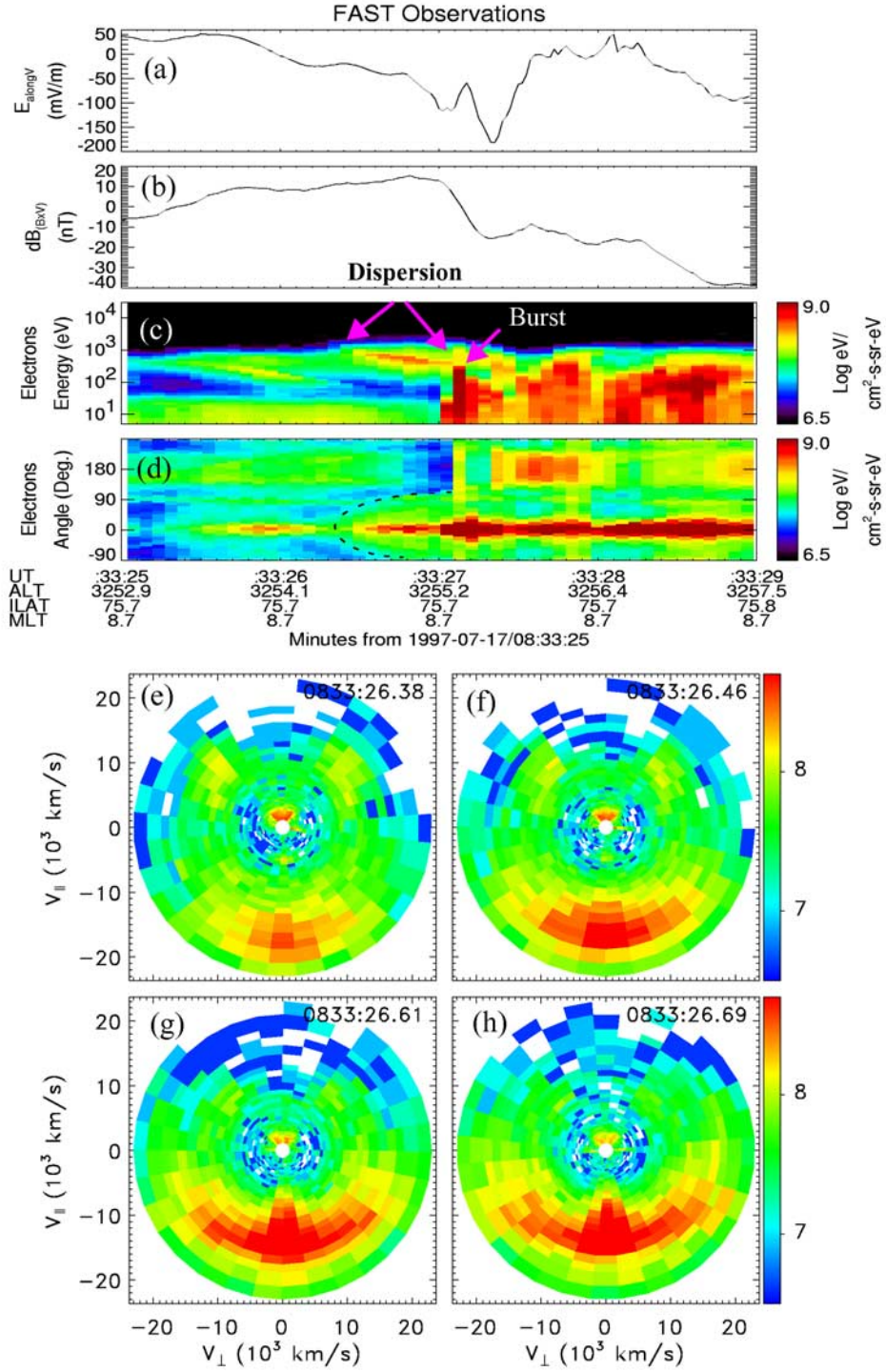

Figure 1. FAST observations of the dayside auroral region on 17 July 1997. (a) Perpendicular electric fields. (b) Perpendicular magnetic fields. (c) Electron energy-time spectrogram. (d) Electron angular time spectrogram, where 0° (180°) indicates the direction parallel (antiparallel) to the local magnetic field. Four snapshots of the electron distribution functions are displayed in Figures 1e–1h during times when the energy-time dispersion signature was observed. The vertical and horizontal axes are parallel and perpendicular velocity with respect to the local magnetic field, where negative velocity is the direction toward the ionosphere. The color represents electron energy fluxes according to the color bar on the right.

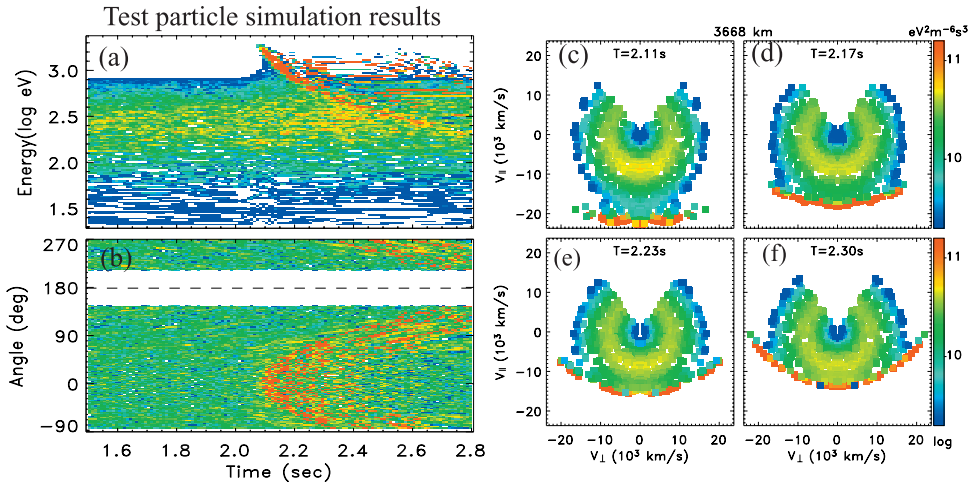

Figure 4. (a) Energy-time and (b) angular-time spectrograms of magnetosheath electrons at 3668 km altitude, where 0° (180°) indicates the direction parallel (antiparallel) to the local magnetic field. Distribution functions of magnetosheath electrons at (c) 2.11, (d) 2.17, (e) 2.23, and (f) 2.30 s.

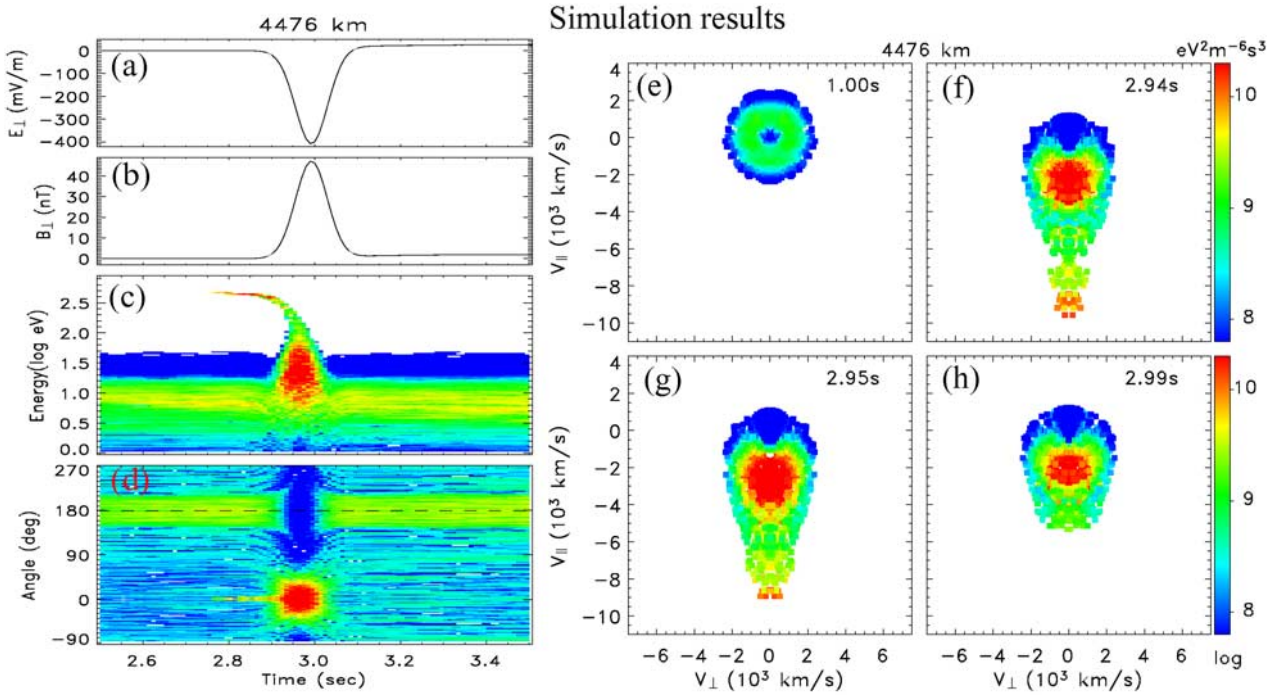

Figure 7. (a) Perpendicular electric and (b) magnetic fields and (c) energy-time and (d) (d) angular-time spectrograms of background electrons at 4476 km altitude. Distribution functions of magnetosheath electrons at times (e) 1.00, (f) 2.94, (g) 2.95, and (h) 2.99 s.